Dielectric Study of the Molecular Mobility and the Isothermal Crystallization Kinetics of an Amorphous Pharmaceutical Drug Substance

J. ALIE,[1] J. MENEGOTTO,[2] P. CARDON,[2] H. DUPLAA,[2] A. CARON,[2] C. LACABANNE,[1] M. BAUER[2]

[1]Polymer Physics Laboratory, CIRIMAT UMR 5085, Université Paul Sabatier, 118 route de Narbonne, 31062 Toulouse Cedex, France

[2]International Analytical Department, Sanofi-Synthelabo Recherche, 195 route d'Espagne, 31036 Toulouse Cedex 04, France

Received 17 February 2003; revised 5 June 2003; accepted 1 July 2003

ABSTRACT: During the development of new pharmaceutical products based on drug substances in their amorphous form, the molecular mobility of an amorphous active ingredient was characterized in detail within a very broad time–temperature range. The relation between the isothermal crystallization kinetics and the dynamics of this amorphous substance was investigated. First, dynamic dielectric spectroscopy (DDS) and the thermostimulated current (TSC) techniques were used to analyze the molecular mobility of the amorphous drug substance over a wide frequency and temperature range (the drug substance is referred to as SSR in this text and was chosen as a model glass-forming system). Two relaxation processes, corresponding to different molecular motions, were identified. The β_a-relaxation process, associated with intramolecular oscillation of small dipolar groups, followed Arrhenius temperature behavior over the entire time–temperature domain that was studied. However, the main α_a-relaxation process, assigned to the dielectric manifestation of the dynamic glass transition of the amorphous phase, was described by Vogel–Fulcher–Tammann (VFT) and Arrhenius behavior above and below the glass transition temperature (T_g) respectively. The physical meaning of these complex dynamics is explained in the context of the Adam and Gibbs (AG) model, by the temperature dependence of the size of cooperatively rearranging regions (CRR) that govern the time scale of delocalized molecular motions. The distinction between the molecular mobility and the structural relaxation of amorphous systems below T_g is discussed. This work shows that the complementary nature of both DDS and TSC techniques is essential to directly analyze the intramolecular and molecular motions of disordered phases over a wide time–temperature range above and below the T_g. Second, real-time dielectric measurements were carried out to determine the isothermal crystallization kinetics of the SSR amorphous drug. Whatever the crystalline form obtained over time in the crystallization process, the decrease of the dielectric response of amorphous phase, which is characteristic of the isothermal crystallization, was studied to monitor the time dependence of the degree of crystallinity. The characteristic crystallization time, derived from Kohlrausch–Williams–Watt (KWW)–Avrami analyses performed at different temperatures, followed an Arrhenius temperature dependence. Behaviors specific to the molecular mobility of the amorphous drug substance were compared with the characteristic crystallization time. It was concluded

Correspondence to: J. Menegotto (Telephone: 33 5 61 16 27 15; Fax: 33 5 61 16 23 64;
E-mail: jerome.menegotto@sanofi-synthelabo.com)

Journal of Pharmaceutical Sciences, Vol. 93, 218–233 (2004)

that the crystal growth process of the SSR drug seems to be controlled by the intramolecular motions involving the β_a-relaxation mode and not by the molecular motions responsible for the α_a-relaxation mode in the range of temperatures $>T_g$. Subsequent studies will focus on the crystallization process of the SSR drug in the glassy state ($T < T_g$). © 2004 Wiley-Liss, Inc. and the American Pharmacists Association J Pharm Sci 93:218–233, 2004

Keywords: amorphous; dynamic dielectric spectroscopy; ThermoStimulated Current; mobility; crystallization; relaxation time; glass transition

INTRODUCTION

The aqueous solubility of new pharmaceutical drug substances is increasingly becoming a concern. If these new drugs have good permeability across the intestinal barrier, then their bioavailability can be improved by promoting the dissolution rate in the gastrointestinal tract. Several different strategies have been adopted to accelerate the dissolution of poorly soluble drugs because the oral route remains the most utilized way to administer a medication. The use of liquid and solid solutions, micronization, and cyclodextrin or other additives are some examples of approaches taken to improve bioavailability. Another possible strategy is to exploit the advantage offered by amorphous phases of a very high free energy state. The latter is characterized by important free volume, which will promote the accessibility of foreign molecules like water and, consequently, the kinetics of dissolution. However, because the molecules in amorphous phases have more free energy, they are more susceptible to chemical reactions leading to impurity formation (toxicity). Equally important is their potential to undergo a crystallization process over time that would potentially impact the bioavailability, which is not pharmaceutically acceptable.

Consequently, the use of amorphous phases has been the subject of very intensive investigations, and this domain, which is already well developed in the study of the physics of solids (especially in the polymer physics area), has moved into the pharmaceutical realm.[1–5] These studies have shown, at least qualitatively, that the molecular mobility of the amorphous phase is responsible for chemical [1,6–8] and physical instabilities.[1,9–12] The physicochemical instabilities of amorphous drugs will remain a great problem until the molecular mobility is well characterized and understood.

The main objective of this study was to investigate the correlation between the molecular mobility of a pure amorphous drug and the kinetics of its isothermal crystallization, which is a major drawback (as already described). In particular, in this work we have attempted to determine which molecular motions are involved in the crystallization process (nucleation, crystal growth).

To reach this goal, the molecular mobility of amorphous drug was detected and analyzed by dynamic dielectric spectroscopy (DDS) and the ThermoStimulated Current technique (TSC), which will be henceforth be collectively referred to as dielectric spectroscopy (DS). Among all techniques currently used to study the dynamics of amorphous phases, such as solid-state nuclear magnetic resonance (NMR), quasi-elastic light scattering (QELS), quasi-elastic neutron scattering (QENS), fluorescence depolarization (FD), differential scanning calorimetry (DSC), dynamic mechanical analysis (DMA), and thermostimulated creep [13] (TSCr), DS was chosen because of its very high sensitivity and its wide accessible frequency range of molecular solicitation. These properties allow detection of motions that have a relaxation time of 10^4–10^{-9} s over a wide temperature range (−160–300°C).[14–17] The main interest in DS is its ability to directly characterize the time scale of intramolecular and molecular motions both above and below the glass transition temperature (T_g) of amorphous phases.[15,16,18] The DSC method is often described in the literature for determination of the molecular mobility of amorphous phase below T_g, by tentatively relating the molecular mobility to the structural relaxation of disordered phases in ageing experiments.[19,20] However, the dielectric techniques directly probe the molecular motions by stimulating the different electrical dipolar groups, with a suitable applied electrical field, thereby allowing a clear differentiation between localized relaxing entities involved in secondary relaxation and the larger sized species involved in the dynamic glass-to-liquid transition.

The crystallization process of amorphous samples has been extensively studied, but most studies reported in the literature are based on analyses performed by optical microscopy under

cross polarizers, X-ray powder diffraction (XRPD), or DSC.[21–23] All these techniques measure the crystal formation from the detection of the specific responses of the crystal (e.g., light polarization, diffraction, and heat of fusion). To determine the kinetics of isothermal crystallization, an original method comprising real-time dielectric measurements was preferred in this work. With this method, the isothermal crystallization of the amorphous sample is monitored *in situ* in the dielectric cell as time elapses, without any temperature change during the entire experiment. In this case, the diminishing dielectric response of the amorphous part is recorded as the increase in degree of sample crystallinity with time.

Analyses of relations between the molecular mobility and the isothermal crystallization kinetics were carried out on a poorly soluble development pharmaceutical drug from the Sanofi-Synthelabo Research Department. This compound, obtained in an amorphous phase and as two different crystalline forms (A and B) that are enantiotropically related, is considered a good model for the study of the propensity of a complex glass-forming system to crystallize over time.

EXPERIMENTAL

Methods

Differential Scanning Calorimetry (DSC)

DSC measurements were carried out with a TA instrument 2920 apparatus, using non-hermetically sealed pans. Thermograms were recorded at a heating rate of 10°C/min from 20 to 180°C, under a dry nitrogen gas purge at a flow rate of 50 mL/min. High purity indium was used for temperature and enthalpy calibration. The glass and the melting transition temperatures were determined as the midpoint of the heat capacity increment and as the onset temperature of the endothermic peak, respectively.

X-ray Powder Diffraction (XRPD)

The XRPD patterns of solid samples were determined at ambient temperature with a Siemens D500TT X-ray powder diffractometer at 40 kV and 25 mA, with CuKα radiation. Counts were measured with a scintillation counter from 4 to 40° in the 2θ diffraction angle range, with an angle rate of change of 1°/min (step size = 0.030°; resi- ; residence time = 2 s).

Dynamic Dielectric Spectroscopy (DDS)

Complex dielectric permittivity ($\varepsilon^* = \varepsilon' - i\varepsilon''$) and dielectric loss factor ($\tan\delta = \varepsilon''/\varepsilon'$) measurements were performed with a Novocontrol (BDS4000) Broadband Dielectric Spectrometer based on an Alpha analyzer. The sample was placed into a dielectric cell especially designed for the analysis of powder and low molecular weight systems exhibiting significant flow at high temperatures. The cell is composed of two electrodes, which are able to follow the geometrical change of a sample, and a Teflon® ring, which keeps the sample between electrodes at high temperatures. The dielectric cell was placed into a cryostat, and the temperature was controlled with an accuracy of $> \pm 0.1$°C by a cold nitrogen gas stream that was heated by a Quatro temperature controller.

To determine the molecular mobility, the dielectric measurements were carried out isothermally from −160 to 150°C in steps of 5°C, in the 10^{-1}–10^6 Hz frequency range. Concerning the isothermal crystallization analyses, *in situ* real-time dielectric measurements were carried out at a given temperature at successive time intervals. For each crystallization temperature, a specific frequency range was selected so that the time of the frequency sweep was short enough to avoid an evolution of the structure of sample. For example, at 120°C, the selected frequency range was between 10^2 and 10^6 Hz so that the corresponding acquisition time of each DDS spectrum was <1 min.

ThermoStimulated Current (TSC)

TSC experiments were carried out with a Thermold® TSC/RMA 9000 instrument. Drug was placed, as for DDS, in a sample cell especially designed for dielectric analyses of powders. Before the experiments were initiated, a secondary vacuum was applied to the sample cell located in the TSC cryostat and subsequently flushed with dry helium. To obtain TSC spectra, the sample was polarized by a static electrical field (E_p = 950 V/mm) at the polarization temperature (T_p) for an amount of time (t_p) that was long enough for the sample to reach the equilibrium polarization. This polarization stage allows the orientation, towards the direction of the field, of dipolar species that are mobile at this temperature. The sample was then quenched to a temperature $T_0 \ll T_p$, which enabled the polarization to be retained. At T_0, the field was switched off, and the sample was short-circuited for a defined amount of time (t_{cc} = 2 min) to remove fast relaxing space charges

and to stabilize the sample temperature. The depolarization current [$I(T)$] was then recorded with a very sensitive electrometer (resolution of 10^{-16}A) as the temperature increased at a constant heating rate of 7°C/min from T_0 to a final temperature (T_f) that was $>T_p$. The variation of the depolarization current versus temperature corresponds to the global TSC spectrum.

Materials

Crystalline Forms of the Drug Substance (SSR)

The drug substance, labeled SSR hereafter, was obtained from Sanofi-Synthelabo Research. This low molecular weight system has been shown to exist in two crystalline forms that are referred to as A and B. Both crystalline forms have low solubility in classical solvents and a good permeation through biomembranes (class 2 in the BCS classification). Consequently, the SSR drug substance represents a good candidate to study for the development of new formulations based on an amorphous drug. Thermograms recorded for the A and B crystalline forms (Fig. 1) display melting transitions characterized by onset temperatures of 146 and 156°C, respectively, and by melting enthalpies of 70 and 58 $J \cdot g^{-1}$, respectively. From these parameters, and from the study of the A and B crystallization in solution at different temperatures, the system was found to be enantiotropic.[24] The solid–solid transition temperature was estimated from thermodynamic values [25] as $\sim T_{ss} =$ 103°C, and the A crystalline form was found to be more stable at temperatures $<T_{ss}$.

Amorphous Form of SSR

The amorphous form of SSR was prepared by melting the A crystalline form of SSR at 180°C for 10 min and then quench cooling the resulting melt in liquid nitrogen. The obtained amorphous film was then ground and stored at 5°C/0% relative humidity (over P_2O_5), despite the substance being hydrophobic. No chemical degradation was observed for the drug substance obtained as amorphous phase by this specific thermal treatment, as determined by high-performance liquid chromatography (HPLC) analyses. The DSC thermogram recorded for the amorphous SSR is shown in Figure 1. The glass transition at $T_g = 76$°C was the single event observed on the thermogram; neither crystallization nor melting transition was noted at high temperature on the thermogram recorded at a heating rate of 10°C/min.

RESULTS

Molecular Mobility of the Amorphous Form of SSR

Dynamic Dielectric Spectroscopy

The dielectric properties of amorphous SSR were recorded isothermally in the 10^{-1}–10^{6} Hz frequency range for temperatures between −160 and 130°C (steps of 5°C). The loss factor [$\tan(\delta) = \varepsilon''/\varepsilon'$] is shown on a logarithmic scale as a function of frequency and temperature in Figure 2. Three

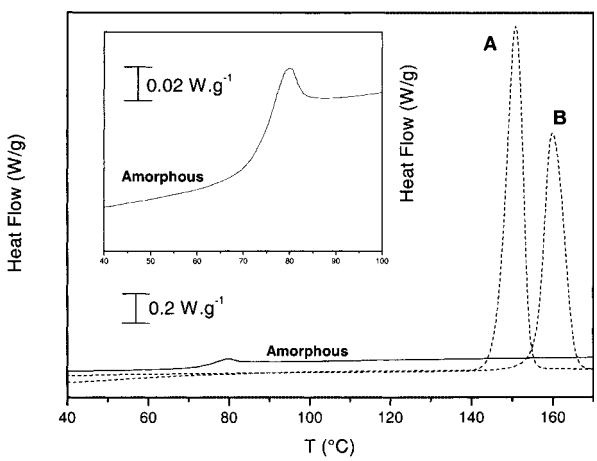

Figure 1. DSC thermograms recorded for SSR in the A and B crystalline forms (dashed lines) and in the amorphous form (solid line). The inset shows an enlargement of the low temperature range.

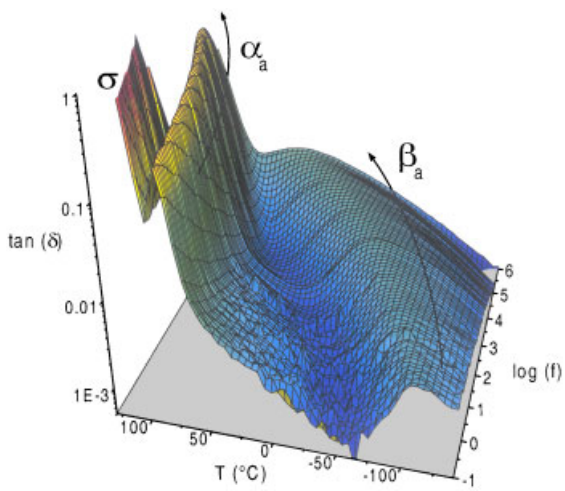

Figure 2. Dielectric loss factor, tan(δ), of the amorphous form of SSR reported on a logarithmic scale as a function of temperature and frequency.

different dielectric events were noted for the amorphous form of SSR. In the low temperature range, a weak and broad relaxation mode was observed. This mode, designated β_a, moved from 10^{-1} to 10^6 Hz as the temperature increased from -155 to 40°C. At high temperature, a more intense and narrow relaxation mode, labeled α_a relaxation, was noted. For sake of clarity, the isothermal DDS spectra, recorded over the 80–130°C temperature range in steps of 10°C, are shown in Figure 3. We note on this figure that the α_a mode extends over the entire accessible frequency range in the temperature range 80–130°C. In the absence of any crystalline phase, the α_a- and β_a-relaxation modes are associated with specific molecular motions of the SSR amorphous phase. In the low frequency and high temperature range, the high values of tan(δ) correspond to the undesired dielectric conductivity, noted as σ, which is due to motions of free electrical charges (electrons or ionic species).

To extract the relaxation time of molecular motions involved in both α_a- and β_a-relaxation modes by taking into account the conductivity phenomenon and the complexity of each mode, all DDS spectra were fitted by a sum of Havriliak–Negami (HN) terms:[26]

$$\varepsilon^*(\omega) = \varepsilon_\infty + \sum_j \frac{\Delta\varepsilon_j}{\left[1 + (i\omega\tau_j)^{\alpha_j}\right]^{\beta_j}} + \frac{\sigma_0}{i\varepsilon_0\omega} \qquad (1)$$

where ε_∞ is the dielectric permittivity at very high frequency; $\Delta\varepsilon_j$ is the dielectric strength; τ_j is the relaxation time; and α_j and β_j are the HN shape parameters ($0 < (\alpha_j;\beta_j) \leq 1$), which describe, respectively, the symmetrical and asymmetrical broadening of the j^{th} relaxation mode ($j = 1$ and 2 for the α_a and β_a relaxations, respectively). The $\sigma_0/(i\omega\varepsilon_0)$ term, where ε_0 is the vacuum dielectric permittivity and σ_0 is the dc conductivity, takes into account the dielectric conductivity phenomenon (σ event). The accuracy of the fit procedure is presented in Figure 3, where HN calculated functions are superimposed on the corresponding DDS experimental points. For each temperature, the fit accuracy coefficient (R^2) is >0.99.

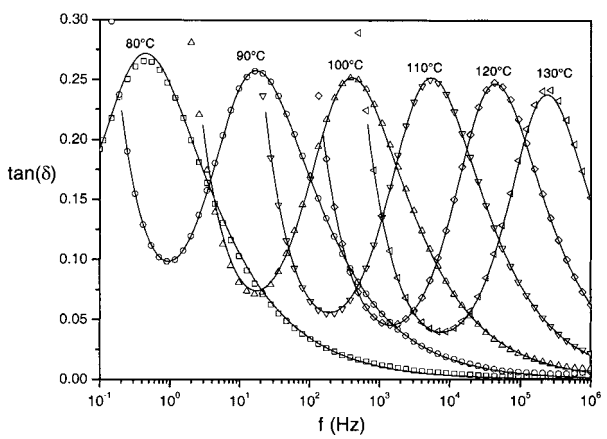

Figure 3. Frequency dependence of the dielectric loss factor, tan(δ), of the amorphous form of SSR recorded at indicated temperatures. Solid lines trace the loss factor calculated from the HN parameters (eq. 1) determined from HN fits of corresponding complex permittivity ε*.

The temperature dependence of HN relaxation times corresponding, respectively, to the α_a- and β_a-relaxation modes, is represented in the Arrhenius diagram shown in Figure 4 (symbols). The temperature dependence of the β_a-relaxation time can be described by Arrhenius behavior:

$$\tau(T) = \tau_{0\alpha} \exp\left(\frac{E}{RT}\right) \qquad (2)$$

where E is the activation energy, τ_{0a} is the pre-exponential factor, and R is the ideal gas constant. In contrast, the α_a-relaxation time follows the Vogel–Fulcher–Tammann (VFT) behavior[17] law:

$$\tau(T) = \tau_{0v} \exp\left(\frac{B}{T - T_0}\right) \qquad (3)$$

where τ_{0v} is the pre-exponential factor and B and T_0 are constants. The different parameters determined from nonlinear least square fit and the associated R^2 values are listed in Table 1. The value of the fragility parameter of the α_a dynamics, $m = 54.7$, was derived from the following expression, which connects the VTF parameters B and T_0 with the fragility index[27] m:

$$m = 16 + \frac{590 \cdot T_0}{B} \qquad (4)$$

In the strong/fragile classification of Angell,[27,28] the m parameter of different liquid glass-forming systems varies from 16 (strong dynamics) to 200 (fragile dynamics) as the intermolecular strengths governing the behavior law of the time scale of molecular motions decrease. From the obtained value of the m parameter, it can be deduced that the amorphous SSR is characterized by weak physical interactions that do not significantly constrain the molecular mobility of this disordered phase.

The VFT behavior law of the α_a-relaxation time unequivocally associates this relaxation mode with the dielectric manifestation of the SSR amorphous phase dynamic glass transition. This assignment is also confirmed by the very good

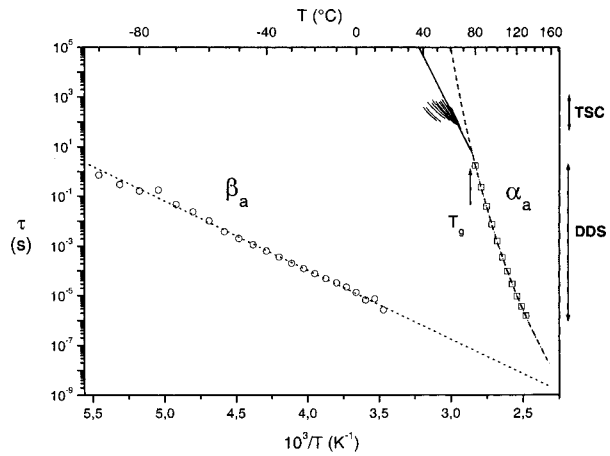

Figure 4. Relaxation time, determined from DDS (symbols) and TSC (short solid lines) analyses, of species involved in the β_a- and α_a-relaxation modes as a function of reciprocal temperature (Arrhenius plot). Solid and dashed lines report Arrhenius and VFT behavior laws characteristic of β_a- and α_a-relaxation modes, respectively.

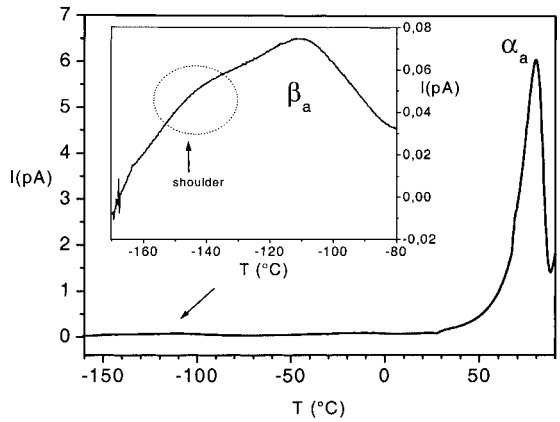

Figure 5. TSC global spectrum of amorphous SSR polarized at 90°C. The inset shows an enlargement of the TSC spectrum recorded in the low temperature range.

agreement noted between the glass transition temperature determined by DSC ($T_g = 76$°C) and the temperature ($T = 74$°C) to which the α_a-relaxation time was extrapolated at 100 s (100 s is the time value that is well known to be the time scale of molecular motions involved in the glass transition at T_g.[28]). The origin of the α_a- relaxation mode is the cooperative motion of the whole of molecules.

The low temperature position and the Arrhenius temperature dependence of β_a-relaxation are characteristic of a secondary dielectric relaxation mode. This relaxation has been attributed to localized intramolecular mobility of SSR molecules on the basis of comparisons with that which has been demonstrated for amorphous and semicrystalline polymers.[13,15–17,29,30] As for polymer materials, the β_a-relaxation process corresponds to the oscillation of small dipolar groups exhibiting relative high dipolar moments.

From DDS measurements, all dynamics specific to the amorphous form of SSR (intramolecular and molecular motions involved in the glass transition) were directly determined in a wide temperature range above and below T_g.

ThermoStimulated Current

The TSC spectrum of the amorphous SSR drug, recorded from −170 to 100°C after polarization of the sample at 90°C, is shown in Figure 5. The inset shows an enlargement of the TSC response recorded at low temperature. Two different relaxation modes were resolved. At high temperature (∼75°C), an intensive and narrow TSC peak was observed. The temperature position of this relaxation mode, very close to the glass transition temperature of amorphous phase detected by DSC, allows us to associate this mode with the dielectric manifestation of the glass transition. This relaxation mode corresponds to the one observed by DDS at high temperature and labeled the α_a-relaxation process. At low temperature (∼−120°C; inset on Figure 5), a very broad and weak relaxation mode was noted. This mode corresponds to the secondary β_a-relaxation process previously observed by DDS.

TSC global spectra obtained from the polarization of the sample at a single high temperature

Table 1. Parameters of Behavior Law of α_a- and β_a-Relaxation Modes of the Amorphous Form of SSR

Relaxation mode	Law	R^2	τ_{0a}; τ_{0v} (s)	E (kJ · mol^{-1})	B (K^{-1})	T_0 (°C)
β_a	Arrhenius	0.998	$8 \cdot 10^{-16}$	53.2	—	—
α_a	VFT	0.9997	$2.8 \cdot 10^{-18}$	—	3926	−15.7

are complex. All relaxation modes detected by the TSC global procedure result from the relaxation of a distribution of relaxing species that differ from each other by their nature and/or their local environment. This fact is evidenced in Figure 5 by the clear shoulder observed on the low temperature side of the β_a-relaxation mode, which corresponds to the relaxation of slightly different dipolar groups from the one involved in the β_a-relaxation mode. This shoulder was observed by TSC and not by DDS because of the very low excitation frequency range of the TSC technique, which increases the resolution of the different relaxation modes by splitting the temperature range in which relevant motions occur.

The fractional polarization technique (TSC-FP) was used to experimentally determine the distribution of different species involved in each relaxation mode with their own dynamics. For this investigation, the sample was polarized within a narrow temperature window ($\Delta T = 5°C$) during the cooling process of the classical TSC thermal program. This polarization window orients only a set of identical species. The TSC-FP elementary spectrum corresponding to the relaxation of selected species was then recorded by the same procedure as that used for the TSC method. By shifting the position of the polarization window along the temperature axis, in steps of 2.5°C, the mobility of all sets of species with different dynamics can be analyzed. Further details regarding the TSC-FP method are available in the literature.[15,18,29,30]

The elementary TSC-FP spectra obtained for the α_a-relaxation mode by shifting the polarization window ($\Delta T = 5°C$) from 45 to 80°C in steps of 2.5°C are plotted in Figure 6. The good agreement between the TSC complex spectrum reported in Figure 5 and the shape of the envelope of all elementary TSC-FP spectra confirms that all different molecular species involved in the α_a-relaxation process were selected by the successive polarization windows.

According to Bucci et al.,[31] the analysis of each elementary TSC-FP spectrum with eq. 5 leads to the temperature dependence of elementary relaxation times, $\tau_{i\,FP}$, which characterizes the dynamics of species involved in the α_a-relaxation mode:

$$\tau_{i\,FP} = \frac{1}{q}\frac{\int_T^{T_f} I_i(T')\mathrm{d}T'}{I_i(T)} \qquad (5)$$

In 5, I_i is the depolarization current of the i^{th} recorded TSC-FP spectrum and q is the heating rate. The temperature dependence of the different elementary relaxation times, $\tau_{i\,FP}$, is shown as a function of reciprocal temperature in Figure 7. All $\tau_{i\,FP}$ exhibit linear behavior on the Arrhenius diagram, which can be described by eq. 2. For each dynamic displayed in Figure 7, the activation parameters were determined from a nonlinear least square fit. The dynamics of relaxing species, which contribute to the α_a-relaxation mode, were characterized by a narrow distribution of activation parameters; the activation energy varies from 103 to 240 $kJ \cdot mol^{-1}$.

Isothermal Crystallization

Before considering the DDS study of the crystallization kinetics of the amorphous SSR, it was important to check that no dielectric response of SSR in the crystalline form interferes with

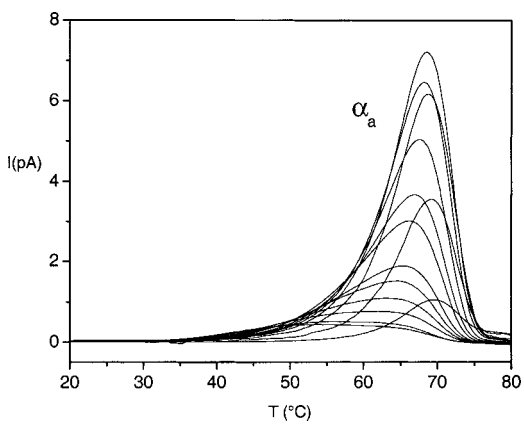

Figure 6. Elementary TSC-FP spectra of the α_a-relaxation mode of the amorphous form of SSR.

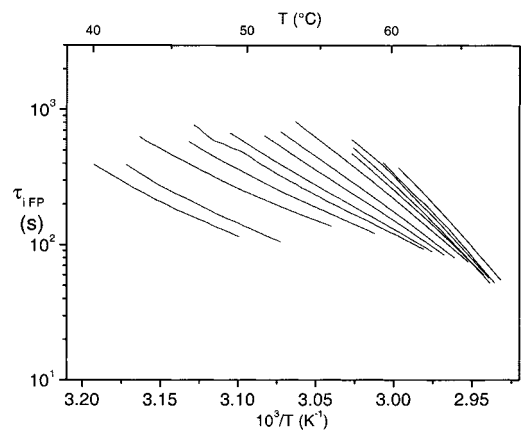

Figure 7. Arrhenius plot of elementary relaxation times $\tau_{i\,FP}$ determined from analyzes of TSC-FP spectra recorded in the α_a temperature range of the amorphous form of SSR.

dielectric responses specific to the amorphous form of SSR. Isothermal DDS spectra for the SSR drug in A crystalline form, recorded from −155 to 130°C in steps of 5°C, are shown in Figure 8. As in the case of the amorphous phase, an important dielectric conductivity was observed in the high temperature and low frequency range. The single relaxation mode that characterizes the A crystalline SSR was observed for high frequencies in the lowest accessible temperature range. This weak relaxation mode, named γ_c, might correspond to oscillations of small dipolar groups located in the crystalline phase that are not inhibited by strong interactions imposed by neighboring molecules. In the entire investigated temperature range, the more-or-less scattered dielectric properties recorded in the 10^{-1}–10^2 Hz frequency range correspond to the dielectric noise associated with the specific detection mode of the dielectric spectrometer used only in this frequency range. This noise is significantly magnified by the large tan(δ) scale adopted in this figure to observe the weak γ_c-relaxation mode. No additional relaxation mode was detected in this frequency range.

It is evident from the results in Figure 8 that the frequency–temperature position of the single weak dielectric relaxation mode detected for SSR in the A crystalline form is outside the range in which the α_a-relaxation mode was detected. This result supports the choice of the α_a-relaxation mode to follow the crystallization of the amorphous form of SSR. Also, this result and the lack of any dielectric event for the A crystalline form of SSR in the α_a-relaxation domain, except the conductivity, show that A crystalline and amorphous dielectric responses are not interfering, thereby confirming that the α_a- and the β_a-relaxation modes are representative of the amorphous state of the SSR. The same conclusion was drawn concerning the B crystalline form with respect to the amorphous phase (data not shown).

The isothermal crystallization of the amorphous SSR was analyzed by real-time *in situ* dielectric measurements performed in the 100–140°C temperature range, in which the α_a-relaxation mode was observed. These experiments correspond to the isothermal cold crystallization of the amorphous SSR because the temperature of the system was increased from room temperature to the temperature of crystallization. As an example, the dielectric properties recorded for SSR, initially in amorphous form, at 120°C in the 10^2–10^6 Hz frequency range for different times between 0 and 41,000 s, are reported in Figure 9 (symbols corresponding to experimental points are not reported here for sake of clarity). It is evident that the intensity of the loss peak (Fig. 9a) and the increment of the real part of the complex permittivity corresponding to the α_a-relaxation mode (Fig. 9b) both decrease as the experiment time increases. These simultaneous phenomena correspond to the isothermal crystallization of the amorphous phase of SSR.

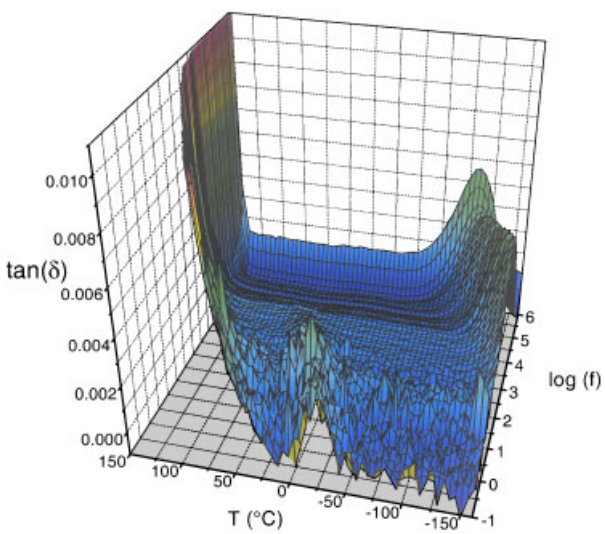

Figure 8. Dielectric loss factor, tan(δ), of SSR in the A crystalline form, reported as a function of temperature and frequency.

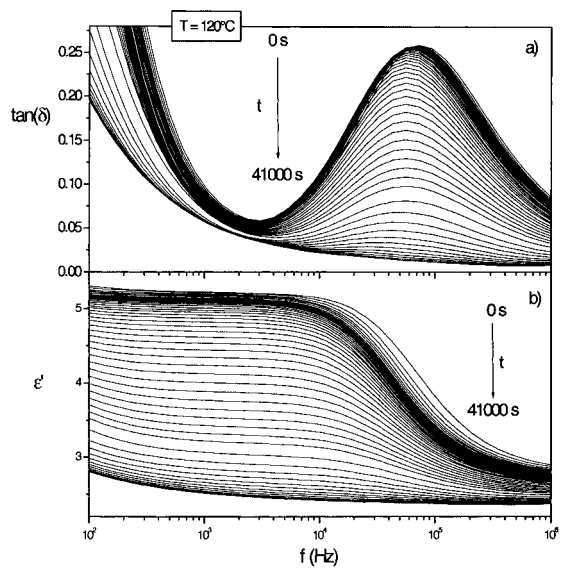

Figure 9. Frequency dependence of isothermal DDS measurements recorded at 120°C for different times: (a) the loss factor tan(δ); (b) real part of the complex permittivity ε′. Arrows displayed on both figures indicate the decreasing signal as the time increases.

The first tan(δ) spectra characterized by high conductivity and the peak positioned at $\sim 6 \cdot 10^4$ Hz and $\tan(\delta)_{max} = 0.26$ correspond to an entirely amorphous sample. After an induction period of time, the intensity of the tan(δ) peak associated with the α_a-relaxation mode decreases with time, indicating crystallization of the amorphous phase. The frequency position and the shape of the α_a-relaxation mode are weakly time dependent. At very long times, the α_a-relaxation is no longer observed, suggesting that conversion of amorphous phase into crystalline phase was completed.

Crystallization was also observed with the real part of the complex permittivity, ε′. During the isothermal crystallization, the intensity of the ε′ increment (i.e., the dielectric strength Δε) decreases continuously with time, whereas its frequency position stays nearly constant. For each spectrum recorded at a selected time, we note also that the ε′ value recorded in the low frequency range is frequency independent. This result indicates that the time needed for each frequency sweep (<1 min for the selected frequency range for experiment performed at 120°C) was short enough to conserve the sample in an isostructural state.

The fact that neither the shape of DDS spectra nor the frequency position of the α_a-relaxation mode evolves very much during crystallization time suggests that the SSR amorphous phase is weakly disturbed by physical constraints imposed by the crystal growth. Depending on the chemical nature of the sample, different results have been reported in the literature regarding this point. For polymers such as poly(ethylene terephthalate)[32,33] and poly(ether ether ketone)[34] that contain rigid backbones, DDS spectra shift to a lower frequency (i.e., the mean relaxation time of the α_a-relaxation mode increases) during the crystallization, indicating that molecular motions in amorphous phases are significantly restricted by the presence of crystallites. In contrast, for low molecular weight systems [35,36] or polymers with flexible chains, such as poly(L-lactic acid),[37] the relaxation time of the α_a-relaxation mode is unaffected by the degree of crystallinity until the crystallinity is high enough to constrain the mobility of amorphous phase. In the latter case, the confinement effect on the amorphous phase appears as the distances between crystallites become shorter than the size of cooperative rearranging regions (CCRs) specific of the amorphous phase at the considered crystallization temperature. The difference between the two kinds of polymers arises from the propensity of each polymer chain to participate simultaneously in both amorphous and crystalline phases.

In the crystallization study described here, the range of interest of the degree of crystallinity is low enough to assume that the confinement effect was ineffective. Therefore, it can be considered that this low molecular weight drug crystallizes in a two-phase system; that is, the system is only composed of amorphous and crystalline zones, which is the ideal one-state model.[18] From this reasonable assumption, the degree of crystallinity of the sample was calculated by the determination of the amorphous content from the intensity of the α_a-relaxation mode.

To extract the crystallization kinetics from dielectric data by taking into account the dielectric conductivity, all isothermal DDS spectra recorded at different times for each crystallization temperature were fitted by the HN expression (eq. 1). For each temperature, the time dependence of the dielectric strength, $\Delta\varepsilon(t)$, of the maximum of the imaginary peak, $\varepsilon''_{max}(t)$, and that of the maximum of the loss factor, $\tan(\delta)_{max}(t)$, were determined and normalized to the corresponding value of the SSR drug in the wholly amorphous state (at $t = 0$). The three normalized parameters were found similar. The time dependence of the degree of crystallinity χ_c for each crystallization temperature between 100 and 140°C was estimated from the normalized dielectric strength[35] according to eq. 6:

$$\chi_c(t) = 1 - \frac{\Delta\varepsilon(t)}{\Delta\varepsilon(t=0)} \tag{6}$$

As expected, the χ_c curves shift to a shorter time as the crystallization temperature increases (see results in Figure 10).

The time evolution of the degree of crystallinity has been often described by the well-known Avrami equation:[38]

$$\chi_c(t) = 1 - \exp(-kt^n) \tag{7}$$

where n and k are the Avrami constants that take into account the mechanism of nucleation and the shape of crystal growth. However, to determine at each temperature a characteristic time for the isothermal crystallization, the Avrami equation has been rewritten here as a phenomenological Kohlraush–Williams–Watts (KWW) equation:[28]

$$\chi_c(t) = 1 - \exp\left[-\left(\frac{t}{\tau_{cr}}\right)^{\beta}\right] \tag{8}$$

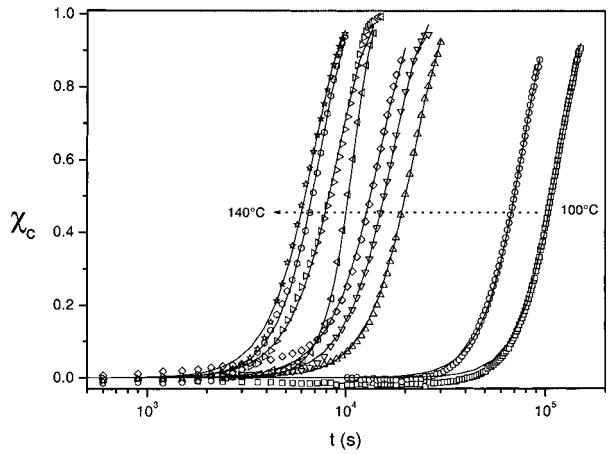

Figure 10. Time dependence of the degree of crystallinity (symbols) of SSR drug during isothermal crystallization performed at different temperatures between 100 and 140°C at steps of 5°C. Solid lines correspond to KWW fit of $\chi_c(t)$ according to eq. 10.

where τ_{cr} is the characteristic crystallization time and β is a constant. These constants are obviously connected to the Avrami parameters by the relationships $\tau_{cr} = k^{-1/n}$ and $\beta = n$.

For each temperature, the characteristic crystallization time was determined from the nonlinear least square KWW fits of the time dependence of the degree of crystallinity. The accuracy of fits ($R^2 > 0.996$) can be seen in Figure 10, where solid lines represent the recalculated time dependence of χ_c.

The temperature dependence of the characteristic crystallization time, τ_{cr}, as a function of reciprocal temperature is shown in Figure 11. A clear trend is noted for the τ_{cr} parameter, and, as expected, the characteristic time is reduced at

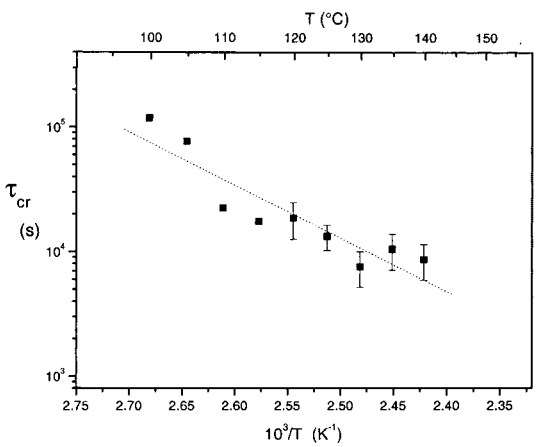

Figure 11. Temperature dependence of the characteristic crystallization time τ_{cr}.

higher temperatures. Even if data points are somewhat scattered due to experimental uncertainties, the temperature dependence of the characteristic crystallization time can be described by Arrhenius behavior (eq. 2) that is characterized by an activation energy of 81.5 $kJ \cdot mol^{-1}$ ($R^2 = 0.91$).

After all isothermal crystallization experiments, the crystallized sample was recovered and gently ground to obtain a fine powder so that its XRPD diffractogram could be recorded at room temperature (data not shown). No amorphous background was noted on the diffractograms acquired for material that had been subjected to any of the employed crystallization temperatures. This result is in agreement with DDS results, indicating that the crystallization was completed after the considered crystallization time. As expected, the B crystalline form was obtained during the isothermal crystallization of the amorphous SSR performed at temperatures >120°C. For temperatures <120°C, a mixture of both A and B crystalline forms was observed, with an increasing A/B ratio as the temperature was decreased. At 100°C, the XRPD spectrum was largely representative of the A crystalline form. These results are in agreement with the theoretically calculated temperature of the solid–solid transition between the two crystalline forms. It is important to note that the temperature dependence of the characteristic crystallization time τ_{cr} was unaffected, whatever the form or the mixture of forms obtained during the isothermal crystallization in the dielectric cell. The latter result is consistent with the physical meaning of τ_{cr}, which represents the characteristic time of the vanishing of amorphous phase during the crystallization and consequently the characteristic time of the global apparition of crystal phases whatever the crystalline form. In this context, the KWW phenomenological expression that is used here to extract a characteristic time for the isothermal crystallization of amorphous phase remains valid for temperatures <120°C, where mixtures of both A and B crystalline forms were observed.

DISCUSSION

Molecular Mobility: Complementary Nature of DDS and TSC Techniques

The molecular mobility specific of the amorphous SSR drug was studied in a wide temperature and frequency range by both DDS and TSC techniques. The temperature dependencies of relaxation

times determined by DDS and TSC were superimposed on the same Arrhenius diagram (Fig. 4). The double vertical arrows on the right-hand side of Figure 4 represent the accessible excitation frequency range of both TSC and DDS experiments. It is evident that the TSC technique allows the study of the dynamics of the sample in the very low frequency range (i.e., a very long time range between 10^2 and 10^4 s).

As already mentioned, the β_a-relaxation mode associated with localized molecular motions involves Arrhenius dynamics over the entire temperature range. The low activation energy and the pre-exponential factor that characterize the β_a-relaxation process (compare with Table 1) are specific to small size species that relax independently from each other. Further experiments based on solid-state carbon-13 nuclear magnetic resonance (^{13}C NMR) measurements have been scheduled to characterize in detail the dipolar groups involved in this relaxation. Some complementary dielectric analyses are also necessary to investigate the distribution of dynamics involved in the β_a-relaxation mode and to thereby access the local density distribution of the SSR amorphous phase.

As shown in Figure 4, at very high temperatures and in the very short time range, the α_a-relaxation time diverges rapidly from the β_a dynamics when the temperature decreases. This phenomenon, currently observed for fragile glass-forming systems and well known as the bifurcation of the $\alpha\beta$ relaxation process,[39,40] is related to the increasing cooperativity specific to molecular motions involved in the α_a-relaxation mode as the temperature decreases. Indeed, when the temperature is reduced, important hindrances affect the larger species involved in the α_a-relaxation, implying their VFT dynamics and thus the observed bifurcation.

Contrary to the dynamics of species implied in secondary β_a-relaxations, which obey Arrhenius behavior over the entire frequency–temperature range probed by TSC and DDS,[15] a change in the dynamics of molecular motions involved in the main α_a-relaxation process of amorphous SSR was noted at T_g (Fig. 12). Indeed, whereas relaxation times derived from the TSC-FP analyses of molecular dynamics involved in the α_a-relaxation process exhibit Arrhenius temperature behavior, that determined by DDS shows VFT temperature dependence. We note that the crossover between the VFT and the Arrhenius behaviors takes place in a temperature range centered around the T_g

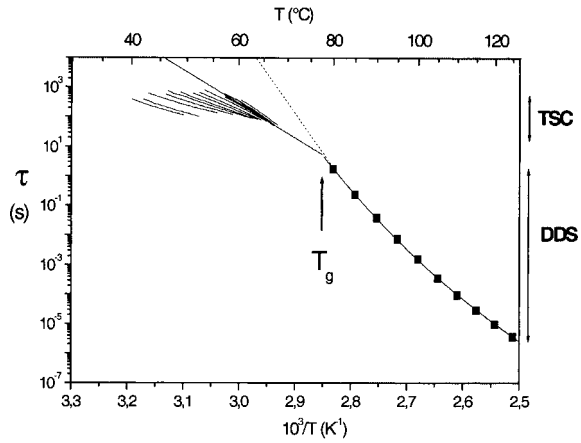

Figure 12. Arrhenius plot of relaxation times determined from DDS measurements (symbols) and from TSC-FP analyses (short solid lines) with their associated behavior laws in time–temperature range in which the α_a-relaxation mode is observed.

detected by DSC and in the time range located around 100 s. The variation of the α_a-relaxation temperature behavior was observed several years ago from mechanical, viscosity, and dielectric measurements on many glass-forming materials.[16,28,41,42] This variation seems to be universal for fragile systems exhibiting VFT temperature behavior for $T > T_g$, and corresponds to the crossover from the equilibrium liquid state (system in a ergodic state for $T > T_g$) to the out-off equilibrium glassy state (system in a nonergodic state for $T < T_g$) when the temperature goes through the thermodynamic glass transition domain. These results (Fig. 12) clearly show the kinetic nature of the dynamic glass transition by showing the change in terms of kinetics law occurring at T_g. In fact, T_g represents the temperature at which the ergodic-to-nonergodic transition takes place by decreasing the temperature.

The physical interpretation of the VFT, the Arrhenius dynamics, and the crossover between them has been made in relation to the Adam and Gibbs (AG) model.[39,42–44] For $T > T_g$, the sharp increase of the apparent activation energy, E (related to $d[\log(\tau)]/d(1/T)$), of the α_a dynamics as the temperature decreases has been explained by a continuous establishment of the cooperativity between the involved molecular motions. In this context, the thermodynamic AG model assumes that amorphous systems comprise a large number of CCRs. These domains, based on species that relax in the same cooperative way, are considered independent from each other. The AG model suggests the following expression for the relaxation

time of species involved in the main α_a-relaxation mode:

$$\tau(T) = \tau_0 \exp\left(\frac{N_A s_c^* \Delta\mu}{k_B T S_c(T)}\right) \quad (9)$$

where $\Delta\mu$ is the individual potential energy barrier; s_c^* is the configurational entropy of the minimum number of species able to rearrange [suggested for polymers to be $s_c^* = k_B \ln(3!)$[45]]; $S_c(T)$ is the macroscopic configurational entropy, which is related to the total number of configurational states accessible to the sample; and N_A is Avogadro's number. Recent work carried out with different techniques shows that the size of CRRs is at a minimum at very high temperature (in the $\alpha\beta$ regime) and increases by coalescence of small CRRs when the temperature decreases to T_g.[39,40,46] The system becomes more and more cooperative, and the configurational entropy [$S_c(T)$] decreases continuously as the temperature decreases.[42,44] Based on experimental observations and on a thermodynamic approach, the following expression of the configurational entropy has been proposed for temperatures $>T$g:[47]

$$S_c(T) = T_g \Delta C_p(T_g) \frac{T - T_0}{T T_0} \quad (10)$$

where $\Delta C_p(T_g)$ is the isobaric heat capacity step at T_g, and T_0 is the temperature at which S_c vanishes, which is referred to in the literature as the Kautzmann temperature. Using eq. 10, eq. 9 for the relaxation time proposed in the AG model can be rewritten as follows:

$$\tau(T) = \tau_0 \exp\left(\frac{N_A S_c^* \Delta\mu T_0}{T_g \Delta C_p T_g k_B (T - T_0)}\right) \quad (11)$$

Equation 11 can take the VFT form (eq. 3) by considering $B = N_A s_c^* \Delta\mu T_0 / (T_g \Delta C_p T_g k_B)$ and $\tau_{0v} = \tau_0$.

At T_g, the cooperativity of molecular motions is so significant that large size CRRs occupy the entire system, which then becomes frozen. The number of CRRs at T_g is at a minimum, and the large volume of CCRs reaches an out-of-equilibrium constant value for temperatures $<T_g$. This situation imposes a constant value, $S_c(T_f)$, for the macroscopic configurational entropy. The value $S_c(T_f)$, which verifies eq. 10, is dependent on the fictive temperature, T_f, introduced by Tool[48] and can only be affected by ageing time applied on the sample in the glassy state before measurements. Below T_g, the relaxation time introduced in the AG model (eq. 9) can then be written as:

$$\tau(T) = \tau_0 \exp\left(\frac{N_A S_c^* \Delta\mu}{k_B T S_c(T_f)}\right) \quad (12)$$

Equation 12 can take an Arrhenius form (eq. 2) by considering that $E = N_A s_c^* \Delta\mu / S_c(T_f)$ and $\tau_{0a} = \tau_0$. This relaxation time corresponds to the time scale of molecular motions involved in the α_a-relaxation mode for the amorphous phase in the glassy state at a given physical ageing state that is taken into account by the fictive temperature T_f. The different relaxation times $\tau_{i\,FP}$ determined by the TSC-FP method below T_g correspond to the time-scale of the relaxing species located in the different CRRs that have different constant size. The TSC-FP method, therefore, can be used to characterize the distribution of constant size CRRs below T_g.

For temperatures $<T_g$, CRRs increase with the ageing time to reach their equilibrium size, which is not acquired during the cooling. The evolution of the size of CRRs is in fact related to the evolution of the environment of relaxing species, which is often referenced as the structural relaxation of amorphous phase. The fictive temperature T_f and the S_c parameter values have decrease with the ageing time.[42,44] From these evolutions, the relaxation time τ of molecular motions then becomes time dependent (through T_f and S_c in eq. 12), and their activation energies [$E = N_A s_c^* \Delta\mu / S_c(T_f)$] increase with the ageing time. The time scale of the evolution of T_f, S_c, or of the relaxation time of molecular motions may be interpreted as the structural relaxation time, τ_r. As described elsewhere,[19,20] the structural relaxation time τ_r can be determined by DSC aging experiments by measuring the enthalpy recovery after storage for different periods at different temperatures. However, the structural relaxation time τ_r cannot be identified as molecular mobility unequivocally related to specific relaxing species. Consequently, the structural relaxation time τ_r determined below T_g and the relaxation time τ of molecular motions involved in the α_a-relaxation mode (Arrhenius or VFT, below and above T_g, respectively) cannot be connected themselves at T_g in the same Arrhenius diagram.

The AG model, almost unanimously accepted to describe the dynamics of glass-forming systems over a wide time–temperature range, gives the physical meaning of dynamics behavior relationships in addition to the VFT–Arrhenius crossover specific to the molecular mobility involved in the α_a-relaxation mode. These results indicate the obvious complementary nature of the DDS and TSC dielectric techniques; that is, DDS allows characterization of the molecular mobility of SSR amorphous phase in the liquid state for

temperatures $>T_g$, and the TSC technique is particularly suitable to study molecular motions in the glassy state for temperatures $<T_g$.

Correlation between Molecular Mobility and Isothermal Crystallization Kinetics

To find a possible correlation between the molecular mobility of the SSR drug substance in amorphous form and the kinetics of its isothermal crystallization, the relaxation time of the different molecular motions specific to the amorphous phase and the characteristic isothermal crystallization time were reported on the same Arrhenius diagram (Fig. 13).

Even if the crystallization time is more affected than the molecular mobility by experimental uncertainties, the first point to be noted from Figure 13 is the significant difference between the VFT dynamics of molecular motions involved in the α_a-relaxation mode at temperatures $>T_g$, and the Arrhenius temperature dependence of the τ_{cr} crystallization time in the same temperature range. This first observation seems to exclude any direct correlation between the α_a-relaxation and the isothermal crystallization kinetics. However, to confirm this conclusion, it is necessary to perform some additional isothermal crystallization measurements below T_g. This approach will, first, increase the analysis temperature range of crystallization analysis and thereby achieve better accuracy for the determination of its behavior, and second, determine if the characteristic crystallization time exhibits a VFT–Arrhenius crossover as is the case for the molecular mobility. For temperatures $<T_g$, the real-time *in situ* DDS measurements appear to be prohibited because of the displacement of the α_a-relaxation mode in a frequency range that is inaccessible for this dynamic experiment. In addition, it is an inefficient use of experimental time to study this temperature range. A new method based on the high resolution of the TSC technique is in development and could avoid this difficulty.

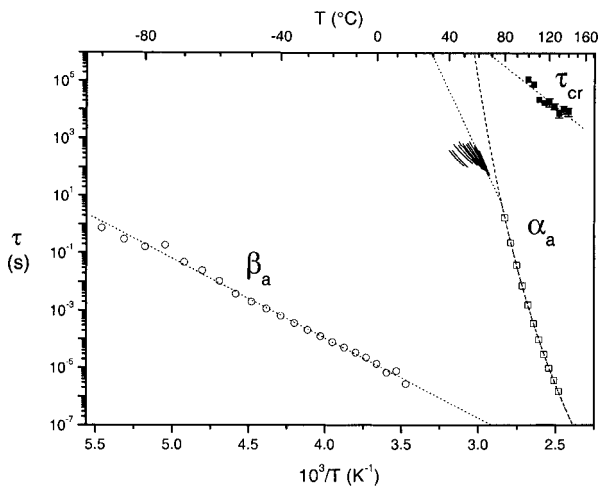

Figure 13. Arrhenius plot of relaxation times associated with the α_a- and β_a-relaxation processes determined by TSC-FP and DDS analyses of the amorphous form of SSR and the temperature dependence of the characteristic crystallization time τ_{cr}. Dotted lines indicate the VFT and Arrhenius behavior laws.

The main interesting point observed in Figure 13 is the connection that can be made between the Arrhenius temperature dependence of the β_a-relaxation mode and the crystallization time τ_{cr}. The dynamics of the β_a-relaxation mode was analyzed by DDS in the -155 to -40°C temperature range. One of the main characteristics of the secondary β_a-relaxation is to keep the same Arrhenius dynamics over the entire range of temperatures (above and below T_g). This behavior is related to the localized nature of involved molecular motions that are unaffected by the glass transition of amorphous phase. The temperature behavior law of the β_a-relaxation time, therefore, can be legitimately extrapolated in the temperature range in which the isothermal crystallization of amorphous phase was analyzed. In the 100–140°C temperature range, the two nearly parallel behavior laws associated with the β_a-relaxation time and the characteristic crystallization time indicate that the molecular motions involved in the β_a-relaxation mode participate in the mechanism of the crystal growth characterized by the crystallization time τ_{cr}. This result suggests that due to their intramolecular motions, molecules localized in the amorphous phase very near to the crystal surfaces can adjust their local conformation to allow their inclusion in the neighboring crystallite. Based on a very different method, a similar conclusion was made by Hikima et al.[23] regarding the isothermal crystallization of triphenylethylene. In this case, the microscopic investigation carried out in the glass transition region showed that the isothermal crystallization was controlled by the molecular motions involved in the β_a-process and not by that involved in the α_a-relaxation mode.

CONCLUSIONS

In the first part of this paper, the molecular mobility of the amorphous form of SSR was

thoroughly analyzed over wide frequency and temperature ranges using both DDS and TSC dielectric techniques. Two relaxation processes, with dynamics specific to glass-forming complex systems, were identified for the amorphous SSR. The secondary β_a-relaxation mode, characterized by Arrhenius behavior over the entire accessible time–temperature range, was associated with intramolecular movements corresponding to oscillations of small dipolar groups that must be identified by solid-state NMR. The dynamics of the main α_a-relaxation process, assigned to the dielectric manifestation of the dynamic glass transition, was described by VFT behavior law at temperatures $>T_g$ and by the Arrhenius law at temperatures $<T_g$. The physical meaning of the VFT and the Arrhenius laws and of the crossover between them at T_g was explained in the context of the AG model by he temperature dependence of the size of CRRs, which govern the time scale of molecular movements involved in the α_a-relaxation mode. DDS and TSC behaved as complementary techniques, giving original information on the intramolecular and molecular mobility in disordered phases over a wide temperature range, above and below T_g.

In the second part of the manuscript, the isothermal crystallization kinetics of the amorphous form of SSR was analyzed at different temperatures with real-time *in situ* dielectric measurements. Whatever the crystalline form obtained from these experiments, the decrease of the dielectric response of the amorphous phase was recorded as a function of time. The characteristic crystallization time was determined by KWW analyses of the time dependence of the degree of crystallinity. The characteristic crystallization time followed an Arrhenius temperature dependence in the supercooled liquid state ($T > T_g$).

Based on the comparison of the behavior laws specific to the molecular mobility of amorphous phase and the characteristic crystallization time, it is concluded that, above T_g, the crystal growth of the SSR is controlled by the intramolecular movements involved in the β_a-relaxation mode independently from the molecular mobility responsible for the α_a-relaxation.

To confirm the correlation observed between the intramolecular mobility of amorphous phases and the crystallization kinetics of these disordered phases, and to thereby highlight the mechanism of crystallization, it would be interesting to explore the temperature range $<T_g$. The aim of this research was obviously to predict the temperature dependence of the crystallization kinetics from the knowledge of the different behavior laws that govern the molecular mobility of amorphous phase. The influence of specific physical interactions with excipients on the molecular mobility of amorphous drugs and the subsequent influence on the crystallization kinetics will be the next fundamental point to be considered in future dielectric investigations. The results of such studies will help in the preparation of specific pharmaceutical formulations that stabilize drugs in the amorphous state, which is well suited to some clinical purposes.

ACKNOWLEDGMENTS

John Alexander, Stephen Byard, and Xavier Fontaine are gratefully acknowledged for their helpful comments and suggestions.

REFERENCES

1. Hancock BC, Zografi G. 1997. Characteristics and significance of the amorphous state in pharmaceutical systems. J Pharm Sci 86:1–12.
2. Hancock BC, Parks M. 2000. What is the true solubility advantage for amorphous pharmaceuticals. Pharm Res 17:397–404.
3. Craig DQM. 1999. The relevance of the amorphous state to pharmaceutical dosage forms: glassy drug and freeze dried systems. Int J Pharm 179:179–207.
4. Kushida I, Ichikawa M, Asakawa N. 2002. Improvement of dissolution and oral absorption of ER-34122, a poorly water-soluble dual 5-lipoxygenase/cyclooxygenase inhibitor with anti-inflammatory activity by preparing solid dispersion. J Pharm Sci 91(1):258–266.
5. Yu L. 2001. Amorphous pharmaceutical solids: preparation, characterization and stabilization. Adv Drug Delivery Rev 48:27–42.
6. Shalaev E, Shalaeva M, Zografi G. 2001. The effect of disorder on the chemical reactivity of an organic solid, tetraglycine methyl ester: Change of the reaction mechanism. J Pharm Sci 91(2):584–593.
7. Lai MC, Hageman MJ, Schowen RL, Borchardt RT, Topp EM. 1999. Chemical stability of peptides in polymers. 1. Effect of water on peptide deamidation in poly(vinyl alcohol) and poly(vinyl pyrrolidone) matrixes. J Pharm Sci 88(10):1073–1080.
8. Lai MC, Hageman MJ, Schowen RL, Borchardt RT, Laird BB, Topp EM. 1999. Chemical stability of peptides in polymers. 2. Discriminating between solvent and plasticizing effects of water on peptide deamidation in poly(vinyl pyrrolidone). J Pharm Sci 88(10):1081–1089.

9. Andronis V, Zografi G. 1998. The molecular mobility of supercooled amorphous indomethacin as a function of temperature and relative humidity. Pharm Res 15(6):835–842.
10. Van den Mooter G, Augustijns P, Kinget R. 1999. Stability prediction of amorphous benzodiazepines by calculation of the mean relaxation time constant using the Williams-Watts decay function. Eur J Pharm Biopharm 48:43–48.
11. Van den Mooter G, Wuyts M, Blaton N, Busson R, Grobet P, Augustijns P, Kinget R. 2001. Physical stabilization of amorphous ketoconazole in solid dispersions with polyvinylpyrrolidone K25. Eur J Pharm Sci 12:261–269.
12. Aso Y, Yoshioka S, Kojima S. 2000. Explanation of the crystallization rate of amorphous nifedipine and phenobarbital from their molecular mobility as measured by ^{13}C nuclear magnetic resonance relaxation time and the relaxation time obtained from the heating rate dependence of the glass transition temperature. J Pharm Sci 90(6):798–806.
13. Doulut S, Demont P, Lacabanne C. 2000. Influence of tacticity on the α retardation mode of poly(methyl methacrylate). Macromolecules 339(9):3425–3430.
14. Kremer F. 2002. Dielectric spectroscopy—yesterday, today and tomorrow. J Non-Cryst Solids 305: 1–9.
15. Menegotto J, Demont P, Bernes A, Lacabanne C. 1999. Combined dielectric spectroscopy and thermally stimulated currents studies of secondary relaxation process in amorphous Poly(ethylene terephthalate). J Polym Sci, Part B: Polym Phys 37:3494–3503.
16. Dantras E, Dudognon E, Samouillan V, Menegotto J, Bernes A, Demont P, Lacabanne C. 2002. Dielectric relaxations in amorphous polymers with complex chain architectures. J Non-Cryst Solids 307(310):671–678.
17. McCrum NG, Read BE, Williams G. 1967. Anelastic and dielectric effects in polymeric solids. London: John Wiley & Sons, Inc., pp 1–617.
18. Boutonnet-Fagegaltier N, Menegotto J, Lamure A, Duplaa H, Caron A, Lacabanne C, Bauer M. 2002. Molecular mobility study of amorphous and crystalline phases of a pharmaceutical product by thermally stimulated current spectroscopy. J Pharm Sci 91, 6:1548–1560.
19. Hancock BC, Shamblin SL, Zografi G. 1995. Molecular mobility of amorphous pharmaceuticals solids below their glass transition temperatures. Pharm Res 12(6):799–806.
20. Di Martino P, Palmieri GF, Martelli S. 2000. Molecular mobility of the paracetamol amorphous form. Chem Pharm Bull 48(8):1105–1108.
21. Yoshioka M, Hancock BC, Zografi G. 1994. Crystallization of indomethacin from the amorphous state below and above its glass transition temperature. J Pharm Sci 83(12):1700–1705.
22. Andronis V, Zografi G. 2000. Crystal nucleation and growth of indomethacin polymorphs from the amorphous state. J Non-Cryst Solids 271:236–248.
23. Hikima T, Hanaya M, Oguni M. 1999. Microscopic observation of a peculiar crystallization in the glass transition region and β-process as potentially controlling the growth rate in triphenylethylene. J Mol Struct 479:245–250.
24. Bauer M. 1999. Le polymorphisme, son origine, ses caractéristiques, ses conséquences dans le domaine pharmaceutique. STP pharm Pra 9(5):354–362.
25. Yu L. 1995. Inferring thermodynamic stability relationship of polymorphs from melting data. J Pharm Sci 84(8):966–974.
26. Havriliak S, Negami S. 1966. A complex plane analysis of α-dispersions in some polymer systems. J Polym Sci, Part C 14:99–117.
27. Böhmer R. 1994. Non-linearity and non-exponentiality of primary relaxations. J Non-Cryst Solids 172–174:628–634.
28. Ediger MD, Angell CA, Nagel SR. 1996. Supercooled liquids and glasses. J Phys Chem 100: 13200–13212.
29. Lacabanne C, Lamure A, Teyssedre G, Bernes A, Mourgues M. 1994. Study of cooperative relaxation modes in complex systems by thermally stimulated current spectroscopy. J Non-Cryst Solids 172–174:884–890.
30. Teyssedre G, Grimau M, Bernes A, Lacabanne C. 1994. α-Relaxation/retardation mode in semicrystalline polymers with flexible chains. Polymer 35:4397–4403.
31. Bucci C, Fieschi R, Guidi G. 1966. Ionic thermocurrents in dielectrics. Phys Rev 148(2):816–823.
32. Fukao K, Miyamoto Y. 1997. Relaxation behavior of α process of poly(ethylene terephthalate) during crystallization process. J Non-Cryst Solids 212: 208–214.
33. Ezquerra TA, Balta-Calleja FJ, Zachmann HG. 1994. Real-time dielectric relaxation of poly(ethylene terephthalate) during crystallization from the glassy state. Polymer 35(12):2600–2606.
34. Nogales A, Ezquerra TA, Denchev Z, Sics I, Balta-Calleja FJ. 2001. Molecular dynamics and microstructure development during crystallization in poly(ether-ether-ketone) as revealed by real-time dielectric and X-ray methods. J Chem Phys 115(8): 3804–3813.
35. Dobbertin J, Hannemann J, Schick C, Pötter M, Dehne H. 1998. Molecular dynamics of the α-relaxation during crystallization of a low molecular weight compound: A real-time dielectric spectroscopy study. J Chem Phys 108(21):9062–9068.
36. Massalska-Arodz M, Williams G, Thomas DK, Jones WJ, Dabrowski R. 1999. Molecular dynamics and crystallization behavior of chiral isooctyloxycyanobiphenyl as studied by dielectric relaxation spectroscopy. J Phys Chem B 103:4197–4205.

37. Mijovic J, Sy JW. 2002. Molecular dynamics during crystallization of poly(L-lactic acid) as studied by broad-band dielectric relaxation spectroscopy. Macromolecules 35:6370–6376.
38. Avrami M. 1941. Kinetics of phase change III: granulation, phase change an microstructures. J Chem Phys 9:177–184.
39. Garwe F, Schönhals A, Lockwenz H, Beiner M, Schröter K, Donth E. 1996. Influence of cooperative α dynamics on local β relaxation during the development of the dynamic glass transition in poly(*n*-alkyl methacrylate)s. Macromolecules 29: 247–253.
40. Schröter K, Unger R, Reissig S, Garwe F, Kahle S, Beiner M, Donth E. 1998. Dielectric spectroscopy in the αβ splitting region of glass transition in poly(ethyl methacrylate) and poly(*n*-butyl methacrylate): Different evaluation methods and experimental conditions. Macromolecules 31:8966–8972.
41. Read BE. 1989. Mechanical relaxation in isotactic polypropylene. Polymer 30:1439–1445.
42. Alegria A, Guerrica-Echevarria E, Goitiandia L, Telleria I, Colmenero J. 1995. α-Relaxation in glass transition range of amorphous polymers. 1. Temperature behavior across the glass transition. Macromolecules 28:1516–1527.
43. Adam G, Gibbs J. 1965. On the temperature dependence of cooperative relaxation properties in glass-forming liquids. J Chem Phys 43(1):139–146.
44. Alegria A, Goitiandia L, Telleria I, Colmenero J. 1997. α-Relaxation in glass transition range of amorphous polymers. 2. Influence of physical aging on the dielectric relaxation. Macromolecules 30:3881–3887.
45. Hodge IM. 1994. Enthalpy relaxation and recovery in amorphous materials. J Non-Cryst Solids 169: 211–266.
46. Donth E. 1996. Characteristic length of the glass transition. J Polym Sci, Part B: Polym Phys 34: 2881–2892.
47. Angell CA, Bressel RD. 1972. Fluidity and conductance in aqueous electrolyte solutions: An approach from the glassy state and the high concentration limit. I. Ca(NO3)2 solutions. J Phys Chem 76:3244–3253.
48. Tool AQJ. 1946. Relation between inelastic deformation and thermal expansion of glass in its annealing range. Ceram Soc 28:240–253.